journal of the mechanical behavior of biomedical materials 126 (2022) 105043

Contents lists available at ScienceDirect

Journal of the Mechanical Behavior of Biomedical Materials

journal homepage: www.elsevier.com/locate/jmbbm

Mechanical modeling of lung alveoli: From macroscopic behaviour to cell mechano-sensing at microscopic level

Gabriel Beltrán [a,b], Daniel Navajas [c,d,e], José Manuel García-Aznar [a,b,*]

[a] Multiscale in Mechanical and Biological Engineering, Department of Mechanical Engineering, Universidad de Zaragoza, Zaragoza, Spain
[b] Aragón Institute of Engineering Research, Zaragoza, Spain
[c] Facultat de Medicina i Ciències de la Salut, Universitat de Barcelona, Barcelona, Spain
[d] Institute for Bioengineering of Catalonia IBEC, The Barcelona Institute of Science and Technology, Barcelona, Spain
[e] CIBER de Enfermedades Respiratorias, Madrid, Spain

A B S T R A C T

The mechanical signals sensed by the alveolar cells through the changes in the local matrix stiffness of the extracellular matrix (ECM) are determinant for regulating cellular functions. Therefore, the study of the mechanical response of lung tissue becomes a fundamental aspect in order to further understand the mechanosensing signals perceived by the cells in the alveoli. This study is focused on the development of a finite element (FE) model of a decellularized rat lung tissue strip, which reproduces accurately the mechanical behaviour observed in the experiments by means of a tensile test. For simulating the complex structure of the lung parenchyma, which consists of a heterogeneous and non-uniform network of thin-walled alveoli, a 3D model based on a Voronoi tessellation is developed. This Voronoi-based model is considered very suitable for recreating the geometry of cellular materials with randomly distributed polygons like in the lung tissue. The material model used in the mechanical simulations of the lung tissue was characterized experimentally by means of AFM tests in order to evaluate the lung tissue stiffness on the micro scale. Thus, in this study, the micro (AFM test) and the macro scale (tensile test) mechanical behaviour are linked through the mechanical simulation with the 3D FE model based on Voronoi tessellation. Finally, a micro-mechanical FE-based model is generated from the Voronoi diagram for studying the stiffness sensed by the alveolar cells in function of two independent factors: the stretch level of the lung tissue and the geometrical position of the cells on the extracellular matrix (ECM), distinguishing between pneumocyte type I and type II. We conclude that the position of the cells within the alveolus has a great influence on the local stiffness perceived by the cells. Alveolar cells located at the corners of the alveolus, mainly type II pneumocytes, perceive a much higher stiffness than those located in the flat areas of the alveoli, which correspond to type I pneumocytes. However, the high stiffness, due to the macroscopic lung tissue stretch, affects both cells in a very similar form, thus no significant differences between them have been observed.

1. Introduction

The extracellular matrix (ECM) stiffness of the lung parenchyma plays a key role in the alveolar cell behaviour and in their critical functions as migration, contraction, cell division and differentiation (Engler et al., 2008; Sunyer et al., 2016; Klein et al., 2009; Mathur et al., 2012; Elosegui-Artola et al., 2017). The lung ECM is subjected to mechanical stretching during breathing, which results in changes in its stiffness due to the strong non-linear mechanical response of this tissue. These changes in the ECM stiffness are sensed by the alveolar cells, regulating their specific cellular behaviour. Therefore, the stiffness of the alveolar cell microenvironment is governed by the macro-scale mechanical state of the lung tissue. In addition, the study of the alteration of matrix mechanics is of particular interest, because it has been proved that it is correlated with severe respiratory diseases (Suki and Bates, 2008; Zhou et al., 2018). ECM stiffening is a hallmark of lung fibrosis (Melo et al., 2014; Ebihara et al., 2000) and alterations in the mechanical properties of the cells' microenvironment have been linked to lung cancer (Puig et al., 2015; Miyazawa et al., 2018; Tilghman et al., 2010; Jeong et al., 2018; Navab et al., 2016).

In the literature, there are different experimental and computational works that have aimed to characterize the mechanical behaviour of lung tissue. So, the macro-mechanical response of the lung tissue has been studied for both tensile (Navajas et al., 1995; Yuan et al., 2000) and compression tests (Andrikakou et al., 2016), while the mechanical response at the micro scale has been mainly studied by means of AFM tests (Luque et al., 2013; Polio et al., 2018). In addition, there are different computer-based models focused on the understanding of the macroscopic behavior of lung mechanics. In these works, different material models were developed, which predict the mechanical response of the lung tissue by defining energy density functions of complex hyperelastic models (Bel-Brunon et al., 2014; Rausch et al., 2011;

* Corresponding author. Multiscale in Mechanical and Biological Engineering, Department of Mechanical Engineering, Universidad de Zaragoza, Zaragoza, Spain.
E-mail address: m2be@unizar.es (J.M. García-Aznar).

https://doi.org/10.1016/j.jmbbm.2021.105043
Received 26 July 2021; Received in revised form 17 November 2021; Accepted 8 December 2021
Available online 14 December 2021

Eskandari et al., 2019) as well as Finite Element (FE) models of the whole lung obtained from CT images in order to analyse the strains during the breathing (Sarabia-Vallejos et al., 2019; Villard et al., 2005; Li and Porikli, 2014). Other works have been based on the reconstruction of the geometry of a network of alveoli by means of simplified models, where the alveoli were modelled by means of regular polyhedra resulting in a homogeneous geometry (Roth et al., 2017; Karami et al., 2017) or even models where the response of a set of alveoli is reproduced using analytical models (BouJawde et al., 2020).

More recently, a combination of computer simulations and experimental measurements have been integrated in order to characterize the multiscale mechanical properties of lung tissue of a rat (Jorba et al., 2019). In this previous work, the micromechanical behaviour of decellularized rat lung tissue was measured experimentally by means of AFM tests. From these experimental results, a hyperelastic material model was defined for simulating the non-linear mechanical response of the ECM lung tissue in the micro scale. The macro mechanical response of decellularized lung was also measured experimentally through tensile tests. The stiffness exhibited by the lung tissue at the macro scale was an order of magnitude lower than that observed at the micro scale. With the support of FE-based simulations, it was concluded that scale-stiffness dependency is due to the highly porous structure presented by the lung tissue. Therefore, the strain supported by the lung tissue during breathing is directly related to the mechano-sensing signals perceived by the alveolar cells through the changes in the local matrix stiffness.

Therefore, in this work we propose a microstructural FE-based model to advance in the understanding of how alveolar cells (type I and type II pneumocytes) are able to sense local stiffness. For this aim, we create a 3D FE model that reproduces the complex and porous microarchitecture of a lung tissue strip, assuming that this microarchitecture is following a 3D Voronoi tessellation. In order to validate this microstructural-based model, we simulate the macroscopic mechanical response corresponding to a tensile test.

2. Materials and methods

In this work, a theoretical multiscale study of the mechanical response of a decellularized rat lung tissue is developed. Therefore, two different models are defined: one corresponding to the macro scale and other to the microstructure. As it will be discussed below, these models are interconnected because the micro-scale model is derived from the macro 3D model of the lung tissue strip.

Thus, this description is based on two main subsections. On the one hand, we create a 3D model that faithfully reproduces the experimental mechanical response obtained for a strip of lung under a tensile test, using a microstructural-based model that recreates its microarchitecture. On the other hand, based on this microstructural model, we simulate the way that alveolar cells are able to perceive the local stiffness as a function of its position in a single alveolus.

2.1. Microstructural-based model following 3D Voronoi tessellation for macroscopic modelling of a uniaxial tensile test

Here we generate a 3D strip lung model that faithfully reproduces both the microstructure of the lung tissue and its mechanical response under an uniaxial tensile test.

The mechanical response of a porous material mainly depends on: 1) the pore microstructure including pore size and pore topology, 2) properties of the bulk material, and 3) the relative density of the material (Markaki and Clyne, 2001). From the previous work (Jorba et al., 2019), the mechanical properties of the bulk lung material were measured by means of AFM tests, and this behavior was modelled trough a hyperelastic Yeoh material model. In this work (Jorba et al., 2019) the average wall thickness and the average diameter of the alveoli were also measured, obtaining a value of 6.6 μm and 50 μm respectively. Therefore, the bulk material, the thickness alveoli wall and the diameter of the alveoli were obtained previously and are considered in the generation of the 3D strip porous lung model.

The lung parenchymal strip structure is an interconnected 3D structure of thin-walled alveoli, which presents a heterogeneous and non-uniform geometrical configuration. Therefore, the three-dimensional model to reproduce the mechanical behaviour of the lung ECM strips must include these particular geometrical characteristics. In this case, we have modelled the macro model of the lung strips by means of a 3D model based on Voronoi tessellation to describe its microarchitecture.

The Voronoi diagram is a mathematical model that consists on the decomposition of a metric space in regions, associated to a cloud of points, in such way that each point is assigned a region of the metric space, formed by the space that is closer to it than to any of the other points (Okabe et al., 2000). This mathematical model is considered very suitable for reproducing the geometry of porous materials with randomly distributed regions (Burtseva et al., 2015; Fantini et al., 2016). In this case, the points on which regions are defined are the geometric centres of the lung alveoli. The methodology used in order to obtain a 3D model based on Voronoi diagram, which reproduces accurately the mechanical response of the lung strip under an axial test, is described below.

The dimensions of the lung strip used in the experimental tensile test were approximately 7x2x2 mm (Jorba et al., 2019). The model corresponding to these dimensions would have implied a very high computational cost, due to the large number of Voronoi regions generated. Therefore, a model with shorter dimensions, but with the same aspect ratio as the original strip, was defined. Thus, the 3D model of the lung tissue specimen consists of a hollow rectangular parallelepiped with 2.8 mm of length, 0.7 mm of width and 0.7 mm of height, which is divided using the Voronoi tessellation (Fig. 1), defining the number of regions (alveoli in this case) in which the model is defined.

In order to estimate the micro-architecture associated to the alveoli of the 3D strip lung model that better predicts the macroscopic behavior of lung tissue, we use an iterative process of trial and error that fits the numerical results to the experimental ones until a minimum criterion error is met. This iterative process consists of the following phases: *1)* Generation of the 3D model based on Voronoi regions, *2)* Mechanical simulation of the tensile test of the lung tissue, and *3)* comparison of the experimental and numerical stress-stretch curve obtained. To evaluate if the numerical results correlates with the experimental data, we compare the R^2 coefficient of determination. If this value is higher than a threshold level (0.95), it means a good fitness of the model. If the coefficient is lower than the threshold, a new analysis is developed and then a new number of Voronoi regions is set and the process is repeated. A scheme of this procedure is shown in Fig. 2.

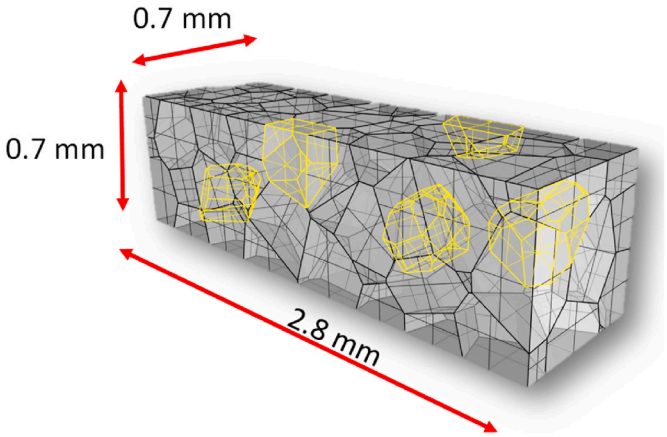

Fig. 1. A hollow rectangular parallelepiped of 2.8x0.7 × 0.7 mm is divided in Voronoi regions in order to generate the 3D model of the lung strip.

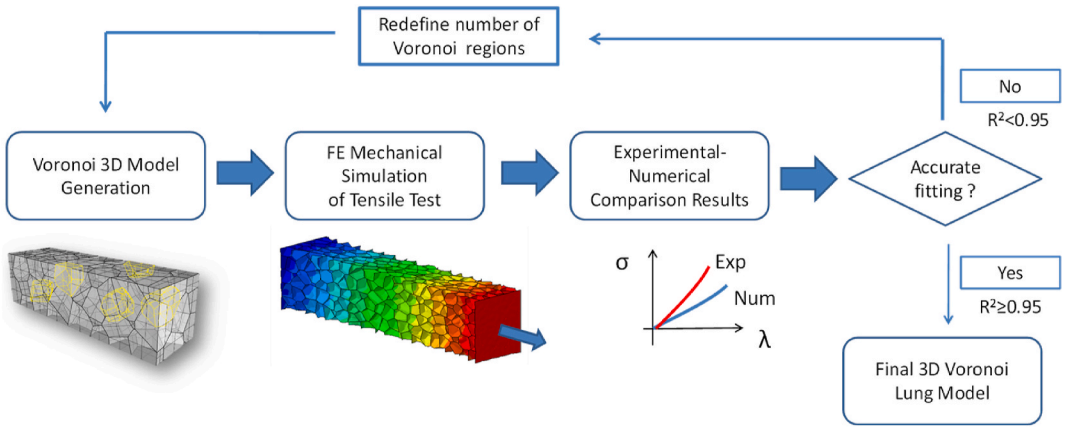

Fig. 2. Scheme of the methodology applied for obtaining a 3D lung strip model based on Voronoi regions. The iterative process of trial and error in order to obtain the 3D lung strip model is based on three phases; 1) Generation of the Voronoi 3D model for a given number of alveoli, 2) Mechanical simulation of the tensile test of the lung strip 3) Evaluation and comparison of the numerical and experimental results. If an accurate fitting is not achieved, a new number of alveoli is defined and a new 3D Voronoi model is generated again.

The first phase of the methodology consists of designing a 3D model of the lung strip based on the Voronoi diagram. The input parameter for the model generation is the number of Voronoi regions, which corresponds to the number of alveoli. In this case, an initial value (starting point) of the number of Voronoi Regions was estimated from an equivalent diameter of 50 μm, which was experimentally measured (Jorba et al., 2019). This initial model showed a higher stiffness under the tensile test than experimentally observed. From the number of alveoli, the 3D model is created using the software *Rhino 6*, which includes a tool that allows to distribute randomly the points, which in this case are the geometrical centres of the alveoli, within a closed volume, and to divide this volume applying the Voronoi tessellation.

In the second phase of the iterative process, a mechanical simulation of the tensile test of the lung tissue strip is performed. The 3D model of the lung string is imported to the commercial software Abaqus and the corresponding finite element (FE) model is defined, including the mesh, boundary conditions and the material model.

Regarding to the FE discretization, the model is meshed with triangular shell elements with a thickness of 6.6 μm, which corresponds to the rat alveolar wall thickness (Jorba et al., 2019) (Perlman and Wu, 2014).

Due to the non-linear mechanical behaviour presented by the lung tissue, an hyperelastic material model is assumed for characterizing its mechanical response. In this case the hyperelastic material model selected is the Yeoh model (Jorba et al., 2019), which strain energy density function is written as:

$$W = \sum_{i=1}^{3} C_{i0}(\overline{I_1} - 3)^i + \frac{1}{D_1}(J_{el} - 1)^2 \tag{1}$$

The first term in Equation (1) corresponds to the or distortional elastic response and the second term to the volumetric (or dilational) elastic response. I_1 is the first deviatoric strain invariant and J the elastic volume ratio. C_{i0} and D_1 are material constants that characterize the isochoric and volumetric elastic response, respectively. The material parameters for the Yeoh model used in the simulations for the lung tissue are summarized in Table 1 (Jorba et al., 2019).

This material model was obtained in a previous work (Jorba et al., 2019), in which the response of lung tissue was characterised at the micro-scale using AFM tests. This characterisation was performed on tissue samples in the order of microns (μm), thus the mechanical behaviour measured corresponds to the local tissue response.

Table 1
Parameters of the Yeoh hyperelastic material model for the lung tissue (Jorba et al., 2019).

C_{10} [kPa]	C_{20} [kPa]	C_{30} [kPa]	D_1 [kPa^{-1}]
1.3	8.9	26.2	0.009

The boundary conditions for numerically simulating the macroscopic tensile test of the lung strip are displayed in Fig. 3.

On the right of Fig. 3, it could be observed that a reference point is defined at one end of the model. The nodes placed at this end of the model are connected to this reference point by means of MPC (Multi-point constrains), thus all the degrees of freedom of the nodes are constrained to this reference point. The axial displacement, u_x, is defined on this reference point while the rest of the displacements and rotations are fixed. The maximum uniaxial displacement u_x applied on the model is 0.6 mm, which corresponds to a deformation of $\varepsilon_x = 21.4\%$. The nodes at the other end (on the left of Fig. 3) remains fixed on X-axis during the simulation.

In order to compare the numerical results with the experimental ones, the axial reaction force (RF_x) and the axial displacement (u_x) are recorded during the simulation. From these parameters the stress (σ) and the stretch (λ) are calculated by means of the following expressions (Equation (2) and Equation (3)):

$$\sigma = \frac{RF_x}{A_0} \tag{2}$$

$$\lambda = \frac{l_0 + u_x}{l_0} \tag{3}$$

where A_0 is the initial cross-sectional area and l_0 is the initial length of the model. In this case the initial length (l_0) is 2.8 mm and the initial cross-sectional area (A_0) is 0.7x0.7 = 0.49 mm^2.

In the third phase of the iterative process, the numerical and experimental curves of *stress (σ) vs. stretch (λ)* are compared. At this point, it should be noticed that experimental results used in this comparison were obtained from tensile tests on rat lung tissue strips in a previous work (Jorba et al., 2019). If the numerical curve does not fit properly with the experimental one, a new number of alveoli is reconsidered and the iterative process starts again in phase 1, generating a 3D model with the new number of Voronoi regions.

Once this process has been carried out for a set of alveoli number, an accurate numerical-experimental correlation was obtained for a number of 1000 Voronoi regions (with a $R^2 = 0.979$), i.e. number of alveoli into which the prism is divided for the model generation. A scheme of the fitting methodology applied in this work is included on the supplementary material section.

From this point, this model based on 1000 Voronoi regions is considered the lung strip 3D model on the macro scale. The 3D lung strip

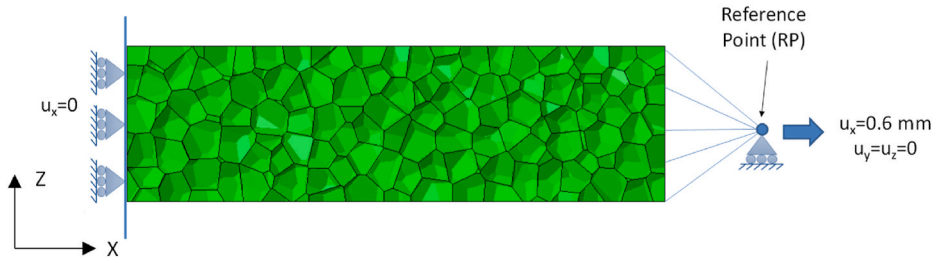

Fig. 3. Boundary conditions applied for reproducing the tensile test of the lung strip. One end of the lung tissue model (left) is fixed on X-axis. On other end, an axial displacement (X-axis) is applied in order to reproduce the tensile test (right).

model was meshed with three-node triangular shell elements. This mesh consists of 819354 elements and 388429 nodes. The simulation of the tensile test was performed in a static single step. A sensitivity analysis of the mesh of this macroscopic model has been developed and the results obtained have been included in the supplementary material section.

2.2. Micromechanical environment of alveoli lung cells simulation

2.2.1. Micromechanical model description

The global strain supported by the lung tissue on the macroscale induces stiffness variations on the ECM due to its non-linear behaviour. These changes in ECM stiffness act as mechanosensing signals "*sensed*" by the lung cells. This process is based on lung cells sensing the mechanical properties of ECM by means of contractile forces through focal adhesions (Kim and Wirtz, 2013), which generate microscale deformations in the surrounding microenvironment. This cell-matrix interplay is what we aim to reproduce by means of the micro model described below.

This micro-model is focused on a few number of alveoli in order to study the micromechanical environment sensed by the alveolar cells at different locations. At this point, it should be noticed that alveolar surface area is mainly covered by two different epithelial cells: type I and type II pneumocytes. Type I pneumocytes are extremely flat and occupy 95% of the surface area of the alveolus, while type II pneumocytes are small cuboidal cells, which usually reside in the corners of the alveolus, covering roughly 2% of the alveolar surface area (Ciechanowicz, 2019).

In this work, two independent factors influencing the stiffness sensed by the alveolar cells are analysed by means of mechanical simulations with the FE micro-model: *i*) the global strain to which the lung tissue is subjected and *ii*) the geometrical position of the lung cell within the alveolus, distinguishing between type I and type II pneumocytes.

The FE micro-model is created from the final 3D model based on Voronoi regions according to subsection 2.1. This simplified model is composed by a few alveoli, which allow to obtain a greater precision in the area of interest and to reduce the computational time (Fig. 4). Due to this simplified model is derived from the 3D Voronoi model, the material properties and the elements in this analysis are the same described in the previous section except in the areas of interest of the adhesion of the cell on the ECM, where a finer mesh has been redefined. The FE micro-model which corresponds to the pneumoctye type I is based on 3245 three-node triangular shell elements, 18358 four-node shell elements and 16733 nodes. For the case of the pneumocyte type II, the FE model is defined by 2772 three-node triangular shell elements, 18344 four-node shell elements and 17050 nodes.

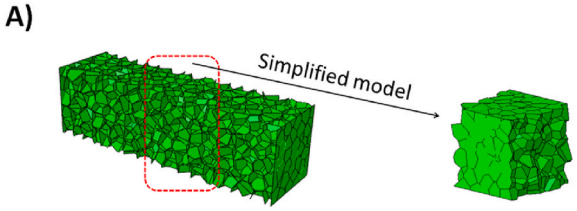

Fig. 4. A simplified model is derived from the fitted Voronoi 3D model.

2.2.2. Mechanical loading

The FE simulations for the micromechanics model are composed by two load steps: *Step 1)* A biaxial deformation is imposed on the micro model in order to reproduce the expansion of the lung tissue during breathing. *Step 2)* Cell contraction is reproduced once the studied deformation level is reached. These two steps are detailed below.

In step 1, the lung expansion is reproduced imposing a perpendicular displacement for each one of the four flat surfaces of the simplified model, resulting in a biaxial deformation on the *YZ* plane. (Fig. 5). These four flat surfaces have been added in order to close the alveoli which were open to the outside in the Voronoi macro model. These flat surfaces allow a better distribution of the reaction forces after imposing the perpendicular displacements and improve the convergence of the analysis. The value of the four displacements is the same within the same case study, $u_z = u_y$, and the level of expansion of the lung tissue is defined as 2^*u_y. In this study are considered four expansion levels: 0 μm, 40 μm, 100 μm and 140 μm, which correspond to the following nominal strains (ε_B): 0%, 5.7%,14.3% and 20%. The displacements are $u_x = 0$ and $u_y = 0$ for the two faces parallel to the XY plane and $u_x = 0$ and $u_z = 0$ for the two faces parallel to the XZ plane. These boundary conditions are summarized on Fig. 5.

Once the lung expansion is simulated in step 1, the cell contraction is simulated on the second step. For this simulation, two study regions have been defined for analyzing the ECM stiffness sensed by the pneumocytes: *1)* flat region, which corresponds to the type I pneumocyte (see Fig. 6A) and *2)* corner region, which corresponds to the type II pneumocyte (see Fig. 6B). These two regions are defined by projecting a circumference of 4.5 μm radius on the surface of the alveolus in the corresponding position. It is assumed that a diameter of 9 μm is representative for both cell types (Young et al., 1991), thus allowing a direct comparison of the results obtained in both regions. It should be remarked that both regions are placed in the same alveoli.

In the step 2 a radial displacement (U_{rad}) is imposed on the circumference projected on the surface of the alveolus in order to reproduce the cell contraction on the ECM. The boundary conditions defined on the step 1 remain fixed in this step, in order to keep the biaxial deformation state reached. The radial displacement of the ECM is defined in the direction of the centre of the projected circumference and its value has been fixed in 0.1 μm, which represents approximately a 1% of the total diameter of the circumference. This aspect is part of hypothesis assumed in this work due to: 1) the difficulty of obtaining experimental data on cell contractions and 2) the main objective is to compare, for the same radial displacement value, the stiffness felt by type I and type II pneumocyte.

At the end of this simulation, the radial reaction forces (RF_{rad}) are evaluated for each study case. A scheme of this step is displayed on Fig. 5.

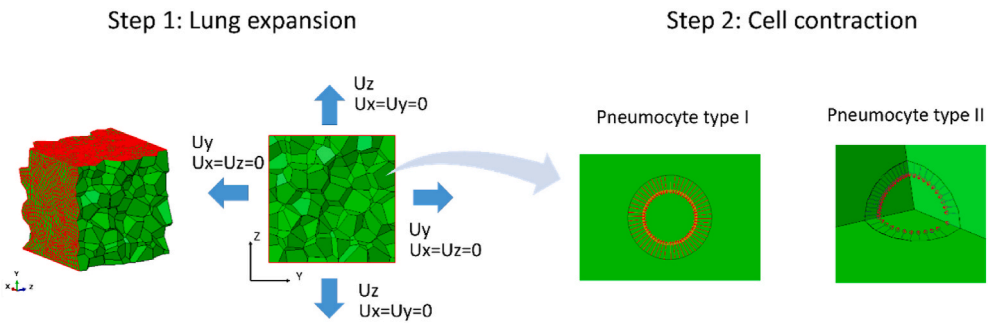

Fig. 5. Step 1: Boundary conditions applied on the micro-model in order to reproduce the lung expansion. Step 2: Boundary conditions applied on the projected circumferences for type I and II pneumocytes. A radial displacement (arrows) on the circumference in the direction of its centre is defined in order to reproduce the radial contraction.

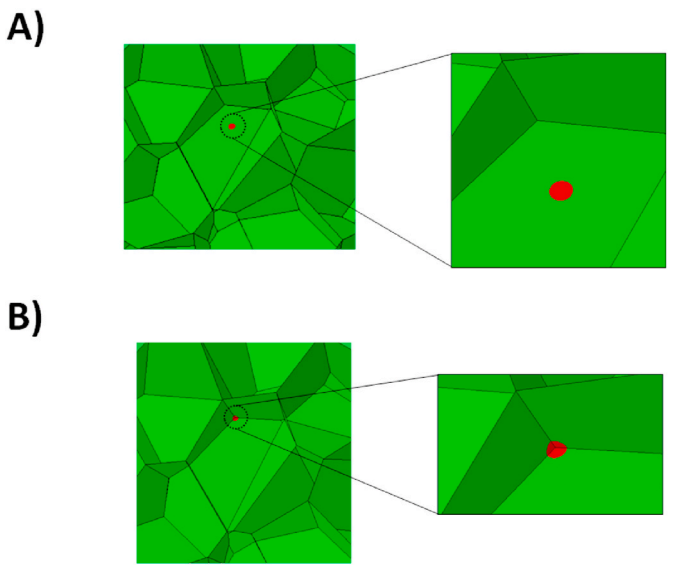

Fig. 6. A) Circumference projected on a flat region of the alveolus for modelling the pneumocyte type I. B) Circumference projected on a corner region of the alveolus for modelling the pneumocyte type II.

3. Results

3.1. Macroscopic model results

The comparison between the numerical and the experimental results for the rat lung tissue strips tensile test is shown in Fig. 7A.

As it can be observed, an accurate numerical-experimental correlation is obtained for the axial mechanical response of the lung strip model. The corresponding alveolus diameter for the case of 1000 Voronoi regions, calculating the volume of an alveolus as the volume of a sphere, is 68 μm.

Measurements of rat lung alveolus diameter have also been evaluated in previous works. In the work of Faffe et al. (2012), the alveolar diameter estimation was 55.8 μm while in the work of Wu et al. (Wu and Perlman, 2012), the value of alveolar diameter obtained was 69 μm. Therefore, the alveolus diameter value of the macroscopic model is very similar to the values experimentally measured.

In Fig. 7B is shown the maximum principal stress distribution [MPa] obtained in the final Voronoi 3D model for an imposed displacement of 0.6 mm.

The porosity of the final model is 84.75%. and the corresponding methodology applied to obtain this porosity value is detailed in Supplementary material section. Experimentally, a tissue fraction ratio of 0.17 has been measured in non-decellularized samples of human lung obtained from autopsy using 3D micro-CT imaging (Kampschulte et al., 2013), i.e. a porosity of 83%. Despite the differences that could exist between the geometry presented by a rat lung and a human lung, the result obtained in the Voronoi model is very consistent with this porosity value. This fact reinforces the idea that the scale dependence of stiffness (between the micro and macro scale) is mainly due to the porous architecture of the lung parenchyma (Jorba et al., 2019).

3.2. Micromechanical model results

The results obtained after the two loads steps obtained for a biaxial strain of $\varepsilon_B = 14.3\%$ (expansion level of 100 μm) are displayed on Fig. 8. The radial displacement (U_{rad}) and the radial reaction force ($\underline{RF}_{rad}$) distribution obtained are shown in Fig. 8A and B for pneumocyte type I and in Fig. 8C and D for pneumocyte type II. It should be remarked that these distributions are projected according to a cylindrical coordinate system, whose origin is located at the geometrical centre of the projected circumference in both pneumocyte types.

As it can be observed, the distribution of maximum principal stress for the type I pneumocyte (Fig. 8B) is significantly more homogeneous than for the type II pneumocyte (Fig. 8D).

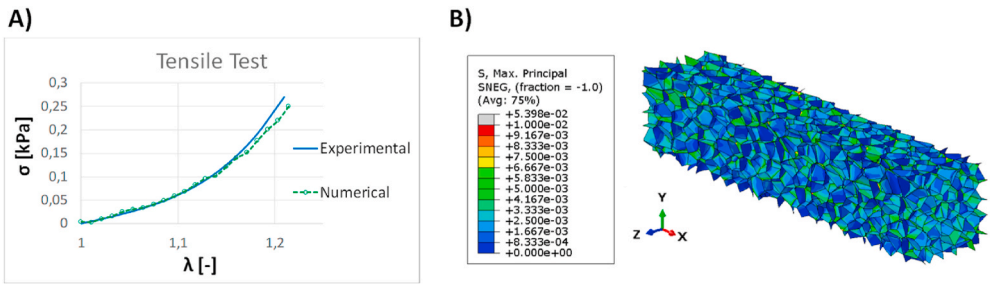

Fig. 7. A) Comparison of stress (σ) vs. stretch (λ) curve for experimental and numerical results. B) Maximum principal stress distribution [MPa] obtained on the Voronoi model.

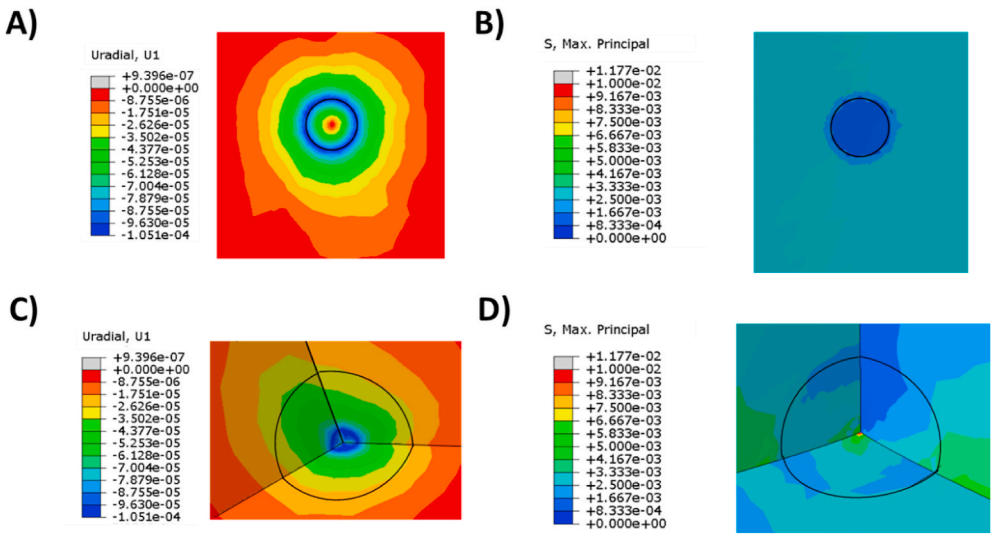

Fig. 8. A) Radial displacement distribution obtained for biaxial strain of $\varepsilon_B = 14.3\%$ in pneumoctyte type I case. B) Maximum principal stress distribution [MPa] obtained for biaxial strain of $\varepsilon_B = 14.3\%$ in pneumoctyte type I case. C) Radial displacement distribution obtained for biaxial strain of $\varepsilon_B = 14.3\%$ in pneumoctyte type II case D) Maximum principal stress distribution [MPa] obtained for biaxial strain of $\varepsilon_B = 14.3\%$ in pneumoctyte type II case.

From the radial reaction forces obtained on each node of the projected circumference at the end of the step 2, the total sum of radial reaction force ($\sum RF_{rad}$), is calculated for each case. In addition, the stiffness sensed by the cell adhered on the ECM, k_{ECM} [N/mm] is defined as follows (Equation (4)):

$$k_{ECM}\ [N/mm] = \frac{\sum RF_{rad}}{U_{rad}} \tag{4}$$

As it has been mentioned above, the radial displacement imposed (U_{rad}) is 0.1 μm for all the cases studied. The cases analysed and the results obtained in terms of the stiffness k_{ECM} are summarized in Table 2 and Table 3 for pneumocyte type I and II correspondingly. For evaluating the evolution of the stiffness k_{ECM} with the biaxial strain (ε_B) for both pneumocyte types, a parameter denoted as *Stiffening Ratio* is defined as follows (Equation (5)):

$$Stiffening\ Ratio_i = \frac{k_{ECMi}}{k_{ECM0}} \tag{5}$$

By means of this parameter is possible to quantify how the stiffness of the extracellular matrix evolves respect to the reference case k_{ECM0}, which corresponds to an unloading biaxial strain of $\varepsilon_B = 0\%$.

Pneumocyte type I Results

Pneumocyte type II Results

The relation between the stiffness of the ECM, k_{ECM} [N/mm] and the biaxial strain [%] is displayed on Fig. 9A for pneumocyte type I and type II while the *stiffening ratio [-] vs. biaxial strain [%]* for both pneumocyte types are compared on Fig. 9B.

This graph on Fig. 9A reveals that stiffness ECM (k_{ECM}) increases exponentially with the biaxial strain for both pneumocyte types. In addition, we can conclude that the stiffness perceived by the type II pneumocyte during the cellular contraction is 1.5–2 times higher than the one sensed by the pneumocyte type I, for the biaxial strain (ε_B) range studied. The results in Fig. 9B reveal that the evolution of the increase in stiffness sensed by the alveolar cells in relation with the biaxial strain is very similar for both types.

A sensitivity analysis of the mesh refinement has been developed, confirming robustness on the achieved results (see Supplementary material section).

Table 2
Evolution of the radial force, stiffness of the ECM and stiffening ratio for each level of biaxial strain studied for pneumocyte type I.

Biaxial Strain, ε_B [%]	F_{radial} [μN]	K_{ECM} [N/mm]	Stiffening Ratio [-]
0	2.49E-02	0.25	1.00
5.7	2.92E-02	0.29	1.19
14.3	7.57E-02	0.76	3.09
20	1.45E-01	1.45	5.44

Table 3
Evolution of the radial force, stiffness of the ECM and stiffening ratio for each level of biaxial strain studied for pneumocyte type II.

Biaxial Strain, ε_B [%]	F_{radial} [μN]	K_{ECM} [N/m]	Stiffening Ratio [-]
0	4.57E-02	0.46	1.00
5.7	5.77E-02	0.58	1.26
14.3	1.17E-01	1.17	2.56
20	2.09E-01	2.09	4.57

4. Conclusions

As a result of this work, a theoretical multiscale model of lung tissue is presented that allows analysing, on the one hand, its macroscopic elastic deformation, and on the other hand, the micromechanical behaviour perceived by the alveolar cells. Therefore, this multi-scale model allows advance in the understanding of how mechanical signals are transmitted from the lung organ to the lung cells through the macroscopic strain and the local stiffness cells sense.

Related to the macro-scale, a 3D model which aims to recreate the alveolar microarchitecture, and the mechanical response under a tensile test of a rat lung strip are obtained. The particular microarchitecture of the lung extracellular matrix, which is based on a network of interconnected alveoli, is modelled using Voronoi regions to reproduce its heterogeneity. The tensile tests are simulated by FE analyses of the 3D Voronoi model obtaining a high numerical-experimental correlation. Therefore, we have obtained a FE model, which reproduces accurately the results of the macro-scale using a material model by characterizing the mechanical response at the micro-scale. Therefore, we can conclude that lung tissue porosity is the property that links both computational analyses. Reinforcing this idea, the porosity of the Voronoi microscopic-based model is very similar to the porosity measured macroscopically in human lungs, with a value around 85% porosity (Kampschulte et al., 2013).

In this micro model, the influence of two independent factors on

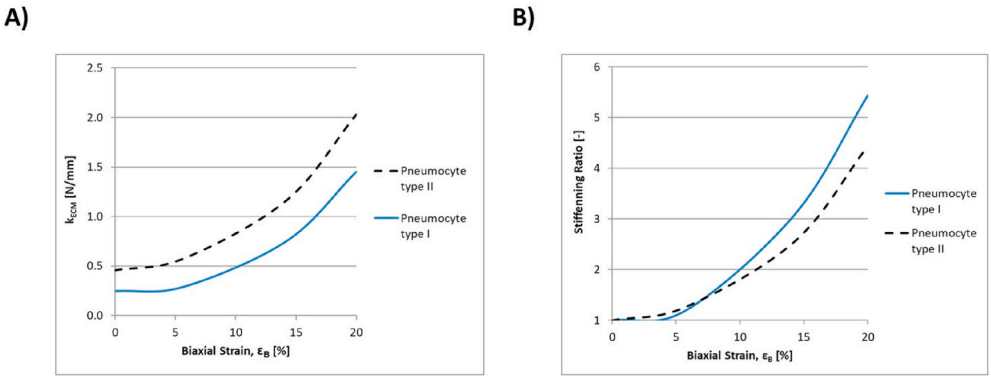

Fig. 9. A) Stiffness ECM (kECM) sensed by both pneumocyte types in relation with the biaxial strain (εB) of the lung tissue. B) Stiffness ratio for both pneumocyte types in relation with biaxial strain (εB) of the lung tissue.

local the stiffness perceived by two main cell types, which cover the surface of the alveolus, have been studied by means of FE-based simulations. These two factors are *i)* the level of global deformation to which the lung tissue is subjected during breathing and *ii)* the position the cells occupy within the alveolus, distinguishing between flat position for type I pneumocytes and corner position for type II pneumocytes. The results of this study reveal that the local stiffness sensed by the cells highly depends on its position in the alveolus. The pneumocytes type II perceive a high local stiffness, from 1.5 to 2 times stiffer than in the case of pneumocytes type I, through the adhesion forces applied on the ECM. In addition, the ECM stiffness perceived by type I pneumocytes has a more homogeneous distribution than the one perceived by type II pneumocytes, because corners act as stress concentrators, resulting in a much more heterogeneous microenvironment in terms of stiffness. The expansion level of lung tissue during breathing also plays an important role in the evolution of ECM stiffness due to its highly non-linear mechanical response. However, the evolution of ECM stiffness is very similar for both types of pneumocytes, taking as a reference the corresponding initial stiffness perceived for each type of pneumocyte, when the tissue is relaxed. Therefore, it can be concluded that the mechanosensory signals regulating cell behaviour are very different for type I and type II pneumocytes due to the geometrical location in the alveoli.

Nevertheless, we have to take into account that our model is based on some assumptions and simplifications, which have to be analysed according to their impact on the results and conclusions obtained. As a first approach, this work is mainly focused on characterizing the elastic response of the lung tissue and its relation with the porosity. However, the characterization of other effects that play an important role in lung tissue mechanics under physiological conditions such as viscoelasticity, plasticity and anisotropy or fluid-structure interaction (Mariano et al., 2020; Chaudhuri et al., 2020) are out of the scope of this work. Hence, these mechanical behaviours will be analysed in future works. We would also like to remark as a simplification of the model that the 3D lung tissue model has been obtained fitting the response under a tensile load until a strain level of ~20%, but other mechanical loads of the lung parenchyma will be studied in future works. In fact, for example Marino et al. (Mariano et al., 2020) have measured strains beyond 30% in some regions of the murine lung.

For the micro-model, the analysis is focused on a single alveolus because the main purpose of this study was to establish a comparison between the perceived stiffness by two types of pneumocytes as a function of their position and the global deformation of the tissue. Therefore, these results are not extensive for all alveoli, since the purpose was to make a first approximation to analyse trends in the stiffness perceived by the alveolar cells. It should be also remarked that the cell contraction has been modelled as a radial displacement, and its value has been estimated in order to establish a comparison between the two pneumocytes types. More complex models that consider a cell model and its interaction with the ECM through simulations modelling contacts and viscoelastic response could be planned for further studies, which would allow a better understanding of mechanosensing signals. A recent work (Panzetta et al., 2019) suggests that cell mechano-sensitivity is regulated by the strain energy of the substrate rather than its stiffness. In this previous study, cells were seeded on linear elastic substrates, and their state was compared as a function of the strain energy of the substrate. This study concluded that the mechanical integrity of the cytoskeleton of cells seeded on stretched substrates was found to be higher compared to those cells seeded on unstretched substrate.

However, in our work the substrate ECM is modelled by means of a hyperelastic material model, thus the stiffness is increasing with the strain energy. Therefore, the increase in terms of stiffness and strain energy of the lung matrix are coupled phenomena, being difficult to distinguish them. Therefore, further investigation is required to unravel how lung cells are able to sense local microarchitecture. Nevertheless, in this work, we successfully show that local stiffness or equivalently strain energy may be the mechanical stimulus that cells use to regulate their location inside the lung ECM. The viscoelasticity of the ECM also plays a key role in the cell-matrix mechano-transduction (Chaudhuri et al., 2020), thus this mechanical response could be characterized in future works with the aim further understanding of this phenomenon.

Consequently, this theoretical multiscale work represents an advance in the understanding of how macroscopic elastic response of the lung tissue is dependent on the porous microarchitecture. Finally, this microstructural model allows to obtain a comparative estimation of how pneumocytes sense their matrix surroundings. For future studies focusing on viscoelasticity and other lung tissue mechanical properties, the multiscale is highly required to further unravel how cells and matrix work together in lung mechanobiology.

Declaration of competing interest

The authors declare that they have no known competing financial interests or personal relationships that could have appeared to influence the work reported in this paper.

Acknowledgements

This work was supported by Spanish Ministry of Economy and Competitiveness [RTI2018-094494-B-C21] and partially financed by the European Union (through the European Regional Development Fund); and the European Union's Horizon 2020 research and innovation programme [826494] and the Marie Skłodowska-Curie grant agreement "Phys2BioMed" [812772].

Appendix A. Supplementary data

Supplementary data to this article can be found online at https://doi.org/10.1016/j.jmbbm.2021.105043.

References

Andrikakou, P., Vickraman, K., Arora, H., 2016. On the Behaviour of Lung Tissue under Tension and Compression. Scientific Reports.

Bel-Brunon, A., Kehl, S., Martin, C., Uhlig, S., Wall, W.A., 2014. Numerical identification method for the non-linear viscoelastic compressible behavior of soft tissue using uniaxial tensile tests and image registration – application to rat lung parenchyma. J. Mech. Behav. Biomed. Mater. 29, 360–374.

Bou Jawde, S., Takahashi, A., Bates, J., Suki, B., 2020. An analytical model for estimating alveolar wall elastic moduli from lung tissue uniaxial stress-strain curves. Front. Physiol. 11.

Burtseva, L., Werner, F., Valdez Salas, B., Pestryakov, A., Romero, R., Petranovskii, V., 2015. Modeling of the Material Structure Using Voronoi Diagrams and Tessellation Methods.

Chaudhuri, O., Cooper-White, J., Janmey, P.A., Mooney, D.J., Shenoy, V.B., 2020. Effects of extracellular matrix viscoelasticity on cellular behaviour. Nature 584, 535–546.

Ciechanowicz, A., 2019. Stem cells in lungs. Adv. Exp. Med. Biol. 1201, 261–274.

Ebihara, T., Venkatesan, N., Tanaka, R., Ludwig, M.S., 2000. Changes in extracellular matrix and tissue viscoelasticity in bleomycin–induced lung fibrosis. Am. J. Respir. Crit. Care Med. 162 (4), 1569–1576.

Elosegui-Artola, A., Andreu, I., Beedle, A.E.M., Lezamiz, A., Uroz, M., Kosmalska, A.J., Oria, R., Kechagia, J.Z., Rico-Lastres, P., Le Roux, A.L., Shanahan, C.M., Trepat, X., Navajas, D., Garcia-Manyes, S., Roca-Cusachs, P., 2017. Force triggers YAP nuclear entry by regulating transport across nuclear pores. Cell 171 (6), 1397–1410.

Engler, A.J., Carag-Krieger, C., Johnson, C.P., Raab, M., Tang, H.Y., Speicher, D.W., Sanger, J.W., Sanger, J.M., Discher, D.E., 2008. Embryonic cardiomyocytes beat best on a matrix with heart-like elasticity: scar-like rigidity inhibits beating. J. Cell Sci. 121, 3794–3802.

Eskandari, M., Nordgren, T.M., O'Connell, G.D., 2019. Mechanics of pulmonary airways: linking structure to function through constitutive modeling, biochemistry, and histology. Acta Biomater. 97, 513–523.

Faffe, D.S., Rocco, P.R.M., Negri, E.M., Zin, W.A., 2012. Comparison of rat and mouse pulmonary tissue mechanical properties and histology. J. Appl. Physiol. 92 (1), 230–234.

Fantini, M., Curto, M., De, F., 2016. CrescenzioA method to design biomimetic scaffolds for bone tissue engineering based on Voronoi lattices. Virtual Phys. Prototyp. 11 (2), 77–90.

Jeong, J., Keum, S., Kim, D., You, E., Ko, P., Lee, J., Kim, J., Kim, J.W., Rhee, S., 2018. Spindle pole body component 25 homolog expressed by ECM stiffening is required for lung cancer cell proliferation. Biochem. Biophys. Res. Commun. 500 (4), 937–943.

Jorba, I., Beltrán, G., Falcones, B., Suki B, B., Farré, R., García-Aznar, J.M., Navajas, D., 2019. Nonlinear elasticity of the lung extracellular microenvironment is regulated by macroscale tissue strain. Acta Biomater. 92, 265–276.

Kampschulte, M., Schneider, C.R., Litzlbauer, H.D., Tscholl, D., Schneider, C., Zeiner, C., Krombach, G.A., Ritman, E.L., Bohle, R.M., Langheinrich, A.C., 2013. Quantitative 3D micro-CT imaging of human lung tissue. Fortschr Röntgenstr 185 (9), 869–876.

Karami, E., Seify, B., Moghadas, H., Sabsalinejad, M., Lee, T.-Y., Samani, A., 2017. Characterizing the Lung Tissue Mechanical Properties Using a Micromechanical Model of Alveolar Sac. Society of Photo-Optical Instrumentation Engineers (SPIE), p. 10137.

Kim, D.-H., Wirtz, D., 2013. Focal adhesion size uniquely predicts cell migration. Faseb. J. 27 (4), 1351–1361.

Klein, E.A., Yin, L., Kothapalli, D., Castagnino, P., Byfield, F.J., Xu, T., Levental, I., Hawthorne, E., Janmey, P.A., Assoian, R.K., 2009. Cell-cycle control by physiological matrix elasticity and in vivo tissue stiffening. Curr. Biol. 19 (18), 1511–1518.

Li, F., Porikli, F., 2014. Biomechanical Simulation of Lung Deformation from One CT Scan, Bio-Imaging and Visualization for Patient-Customized Simulations, pp. 15–29.

Luque, T., Melo, E., Garreta, E., Cortiella, J., Nichols, J., Farre, R., Navajas, D., 2013. Local micromechanical properties of decellularized lung scaffolds measured with atomic force microscopy. Acta Biomater. 9 (6), 6852–6859.

Mariano, C.A., Sattari S, S., Maghsoudi-Ganjeh, M., Tartibi, M., Lo, D.D., Eskandari, M., 2020. Novel mechanical strain characterization of ventilated ex vivo porcine and murine lung using digital image correlation. Front. Physiol. 11, 600492.

Markaki, A., Clyne, B., 2001. The effect of cell wall microstructure on the deformation and fracture of aluminum-based foams. Acta Mater. 49, 1677–1686.

Mathur, A., Moore, S.W., Sheetz, M.P., Hone, J., 2012. The role of feature curvature in contact guidance. Acta Biomater. 8 (7), 2595–2601.

Melo, E., Cardenes, N., Garreta, E., Luque, T., Rojas, M., Navajas, D., Farre, R., 2014. Inhomogeneity of local stiffness in the extracellular matrix scaffold of fibrotic mouse lungs. J. Mech. Behav. Biomed. Mater. 37, 186–195.

Miyazawa, A., Ito, S., Asano, S., Tanaka, I., Sato, M., Kondo, M., Hasegawa, Y., 2018. Regulation of PD-L1 expression by matrix stiffness in lung cancer cells. Biochem. Biophys. Res. Commun. 495 (3), 2344–2349.

Navab, R., Strumpf, D., To, C., Pasko, E., Kim, K.S., Park, C.J., Hai, J., Liu, J., Jonkman, J., Barczyk, M., Bandarchi, B., Wang, Y.H., Venkat, K., Ibrahimov, E., Pham, N.A., Ng, C., Radulovich, N., Zhu, C.Q., Pintilie, M., Wang, D., Lu, A., Jurisica, I., Walker, G.C., Gullberg, D., Tsao, M.S., 2016. Integrin alpha11beta1 regulates cancer stromal stiffness and promotes tumorigenicity and metastasis in non-small cell lung cancer. Oncogene 35 (15), 1899–1908.

Navajas, D., Maksym, G.N., Bates, J.H.T., 1995. Dynamic viscoelastic nonlinearity of lung parenchymal tissue. J. Appl. Physiol. 79 (1), 348–356.

Okabe, A., Boots, B., Sugihara, K., 2000. Spatial Tessellations: Concepts and Applications of Voronoi Diagrams, second ed. Wiley, New York.

Panzetta, V., Fusco, S., Netti, P.A., 2019. Cell mechanosensing is regulated by substrate strain energy rather than stiffness. Proc. Natl. Acad. Sci. Unit. States Am. 116 (44), 22004–22013.

Perlman, C.E., Wu, Y., 2014. In situ determination of alveolar septal strain, stress and effective Young's modulus: an experimental/computational approach. Am. J. Physiol. 307, 302–310.

Polio, S.R., Kundu, A.N., Dougan, C.E., Birch, N.P., Aurian-Blajeni, D.E., Schiffman, J.D., Crosby, A.J., Peyton, S.R., 2018. Cross-platform mechanical characterization of lung tissue. PLoS One 13 (10).

Puig, M., Lugo, R., Gabasa, M., Giménez, A., Velásquez, A., Galgoczy, R., Ramírez, J., Gómez-Caro, A., Busnadiego, Ó., Rodríguez-Pascual, F., Gascón, P., Reguart, N., Alcaraz, J., 2015. Matrix stiffening and b1 integrin drive subtype-specific fibroblast accumulation in lung cancer. Mol. Cancer Res. 13 (1), 161–173.

Rausch, S.M.K., Martin, C., Bornemann, P.B., Uhlig, S., Wall, W.A., 2011. Material model of lung parenchyma based on living precision-cut lung slice testing. J. Mech. Behav. Biomed. Mater. 4 (Issue 4), 583–592.

Roth, C.J., Yoshihara, L., Wolfgang, A.W., 2017. A simplified parametrised model for lung microstructures capable of mimicking realistic geometrical and mechanical properties. Comput. Biol. Med. 89, 104–114.

Sarabia-Vallejos, M.A., Zuñiga, M., Hurtado, D.E., 2019. The role of three-dimensionality and alveolar pressure in the distribution and amplification of alveolar stresses. Sci. Rep. 19 (8783).

Suki, B., Bates, J.H.T., 2008. Extracellular matrix mechanics in lung parenchymal diseases. Respir. Physiol. Neurobiol. 163, 33–43.

Sunyer, R., Conte, V., Escribano, J., Elosegui-Artola, A., Labernadie, A., Valon, L., Navajas, D., García-Aznar, J.M., Muñoz, J.J., Roca-Cusachs, P., Trepat, X., 2016. Collective cell durotaxis emerges from long-range intercellular force transmission. Science 353 (6304), 1157.

Tilghman, R.W., Cowan, C.R., Mih, J.D., Koryakina, Y., Gioeli, D., Slack-Davis, J.K., Blackman, B.R., Tschumperlin, D.J., Parsons, J.T., 2010. Matrix rigidity regulates cancer cell growth and cellular phenotype. PLoS One 5 (9).

Villard, P., Beuve, M., Shariat, B., Baudet, V., Jaillet, F., 2005. Simulation of Lung Behaviour with Finite Elements: Influence of Bio-Mechanical Parameters. Third International Conference on Medical Information Visualisation-BioMedical Visualisation, pp. 9–14.

Wu, Y., Perlman, C.E., 2012. In situ methods for assessing alveolar mechanics. J. Appl. Physiol. 519–526, 1985.

Young, S.L., Fram, E.K., Spain, C.L., Larson, E.W., 1991. Development of type II pneumocytes in rat lung. Am. J. Physiol. 260 (2 Pt1).

Yuan, H., Kononov, S., Cavalcante, F.S.A., Lutchen, K.R., Ingenito, E.P., Suki, B., 2000. Effects of collagenase and elastase on the mechanical properties of lung tissue strips. J. Appl. Physiol. 89 (1), 3–14.

Zhou, Y., Horowitz, J.C., Naba, A., Ambalavanan, N., Atabai, K., Balestrini, J., Bitterman, P.B., Corley, R.A., Ding, B.-S., Engler, A.J., Hansen, K.C., Hagood, J.S., Kheradmand, F., Lin, Q.S., Neptune, E., Niklason, L., Ortiz, L.A., Parks, W.C., Tschumperlin, D.J., White, E.S., Chapman, H.A., Thannickal, V.J., 2018. Extracellular matrix in lung development, homeostasis and disease. Matrix Biol. 77–104.